UNIVERSITÀ DI SIENA 1240

USiena

Novel spiroindoline HDAC inhibitors: Synthesis, molecular modelling and biological studies

This is the peer reviewed version of the following article:

Original:

Brindisi, M., Senger, J., Cavella, C., Grillo, A., Chemi, G., Gemma, S., et al. (2018). Novel spiroindoline HDAC inhibitors: Synthesis, molecular modelling and biological studies. EUROPEAN JOURNAL OF MEDICINAL CHEMISTRY, 157, 127-138 [10.1016/j.ejmech.2018.07.069].

Availability:

This version is availablehttp://hdl.handle.net/11365/1058108 since 2018-11-08T12:44:29Z

Published:

DOI:10.1016/j.ejmech.2018.07.069

Terms of use:

Open Access

The terms and conditions for the reuse of this version of the manuscript are specified in the publishing policy. Works made available under a Creative Commons license can be used according to the terms and conditions of said license.
For all terms of use and more information see the publisher's website.

(Article begins on next page)

25 April 2025

Accepted Manuscript

Novel spiroindoline HDAC inhibitors: Synthesis, molecular modelling and biological studies

Margherita Brindisi, Johanna Senger, Caterina Cavella, Alessandro Grillo, Giulia Chemi, Sandra Gemma, Dora Mariagrazia Cucinella, Stefania Lamponi, Federica Sarno, Concetta Iside, Angela Nebbioso, Ettore Novellino, Tajith Baba Shaik, Christophe Romier, Daniel Herp, Manfred Jung, Stefania Butini, Giuseppe Campiani, Lucia Altucci, Simone Brogi

PII: S0223-5234(18)30634-2

DOI: 10.1016/j.ejmech.2018.07.069

Reference: EJMECH 10604

To appear in: *European Journal of Medicinal Chemistry*

Received Date: 21 March 2018

Revised Date: 27 July 2018

Accepted Date: 29 July 2018

Please cite this article as: M. Brindisi, J. Senger, C. Cavella, A. Grillo, G. Chemi, S. Gemma, D.M. Cucinella, S. Lamponi, F. Sarno, C. Iside, A. Nebbioso, E. Novellino, T.B. Shaik, C. Romier, D. Herp, M. Jung, S. Butini, G. Campiani, L. Altucci, S. Brogi, Novel spiroindoline HDAC inhibitors: Synthesis, molecular modelling and biological studies, *European Journal of Medicinal Chemistry* (2018), doi: 10.1016/j.ejmech.2018.07.069.

This is a PDF file of an unedited manuscript that has been accepted for publication. As a service to our customers we are providing this early version of the manuscript. The manuscript will undergo copyediting, typesetting, and review of the resulting proof before it is published in its final form. Please note that during the production process errors may be discovered which could affect the content, and all legal disclaimers that apply to the journal pertain.

ACCEPTED MANUSCRIPT

Graphical abstract

Novel Spiroindoline HDAC inhibitors: Synthesis, Molecular Modelling and Biological Studies

ACCEPTED

ACCEPTED MANUSCRIPT

Novel Spiroindoline HDAC inhibitors: Synthesis, Molecular Modelling and Biological Studies

Margherita Brindisi[a], Johanna Senger[b], Caterina Cavella[a], Alessandro Grillo[a], Giulia Chemi[a], Sandra Gemma[a], Dora Mariagrazia Cucinella[a], Stefania Lamponi[a], Federica Sarno[c,d], Concetta Iside[c,d], Angela Nebbioso[c,d], Ettore Novellino[e], Tajith Baba Shaik[f], Christophe Romier[f], Daniel Herp[b], Manfred Jung[b], Stefania Butini[a,], Giuseppe Campiani[a,**], Lucia Altucci[c,d], Simone Brogi[a]*

[a]*European Research Centre for Drug Discovery and Development (NatSynDrugs) and Department of Biotechnology, Chemistry, and Pharmacy, Department of Excellence 2018-2022, University of Siena, via Aldo Moro 2, 53100 Siena, Italy.*
[b]*Institute of Pharmaceutical Sciences, Albert-Ludwigs-Universität Freiburg, Albertstraße 25, 79104 Freiburg, Germany.*
[c]*Department of Biochemistry, Biophysics & General Pathology, Second University of Napoli, Vico Luigi De Crecchio 7, 80138 Napoli, Italy.*
[d]*Institute of Genetics and Biophysics Adriano Buzzati-Traverso, IGB-CNR, Via Pietro Castellino 111, 80131 Napoli, Italy.*
[e]*Department of Pharmacy, University of Napoli Federico II, Via D. Montesano 49, 80131 Napoli, Italy.*
[f]*Département de Biologie Structurale Intégrative, Institut de Génétique et Biologie Moléculaire et Cellulaire (IGBMC), Université de Strasbourg (UDS), CNRS, INSERM, 67404 Illkirch Cedex, France*

Keywords

Antitumor agents, bioinformatics, drug design, enzyme inhibitors, epigenetics, HDAC

Corresponding Authors:

*Stefania Butini, Tel. +390577234161, email: butini3@unisi.it

**Giuseppe Campiani, Tel. +390577234172, email: campiani@unisi.it

ACCEPTED MANUSCRIPT

ACCEPTED MANUSCRIPT

Abstract

This paper describes the rational development of a series of novel spiroindoline derivatives endowed with selective inhibitory activity on the HDAC6 isoform. A convenient multicomponent *one-pot* protocol was applied for the assembly of the desired *N*1-substituted spiroindoline core which allowed a straightforward analoging. Computational studies and *in vitro* determination of inhibitory potency for the developed compounds against HDAC6 and HDAC1 isoforms were flanked by cell-based studies on histone H3 and α-tubulin acetylation. The effects on cancer cell cycle and apoptosis of the best performing derivatives were assessed on cancer cell lines highlighting a promising antitumor potential. In view of cell-based data and calculated drug-like properties, the selective HDAC6 inhibitor **5b**, with a spiroindoline-based hydroxamate bearing a *tert*-butyl carbamate functionality, was selected to be further investigated for its potential in inhibiting tumor cells migration. It was able to potently inhibit cell migration in SH-SY5Y neuroblastoma cells and did not display toxicity in NIH3T3 mouse fibroblasts. Taken together, these data foster further investigation and optimization for this class of compounds as novel anticancer agents.

ACCEPTED MANUSCRIPT

ACCEPTED MANUSCRIPT

1. Introduction

In the past decades, histone deacetylases (HDACs) have emerged as versatile therapeutic targets. Histones deacetylation process causes a variation of the chromatin structure thus enabling the accessibility of transcription factors to their target genes, including tumor suppressor genes or oncogenes [1, 2]. The abnormal modulation of this process can influence tumor progression [3] and can also be involved in a variety of neurological disease states, tissue fibrosis, autoimmune and inflammatory diseases, and metabolic disorders [4, 5]. Based on these evidences, HDAC inhibitors (HDACi) gained increasing interest as promising agents for treating several diseases. Regarding their anticancer potential, HDACi were demonstrated to induce cell cycle arrest, apoptosis and tumor growth decrease [6]. For this purpose, the Food and Drug Administration (FDA) has recently approved a series of HDACi for the treatment of different types of cancers. In particular, Vorinostat (**1**, Figure 1) was licensed in 2006 for the treatment of refractory cutaneous T-cell lymphoma (CTCL) [7], Romidepsin (**2**, Figure 1) was approved in 2009 for the treatment of CTCL and in 2011 for treating peripheral T-cell lymphoma (PTCL) [8], Belinostat (**3**, Figure 1) licensed in 2014 for the treatment of PTCL [9], and in 2015 Panobinostat (**4**, Figure 1) was approved for the treatment of recurrent multiple myeloma [10]. Other HDACi such as Mocetinostat (MGCD0103) [11], Abexinostat (PCI-24781) [12], Entinostat (MS-275) [13], Givinostat (ITF2357) [14] and Ricolinostat (ACY-1215) [15] are currently undergoing clinical trials for various types of cancers [16]. Moreover, Tucidinostat (Chidamide) was recently approved by Chinese FDA to treat PTCL [17].

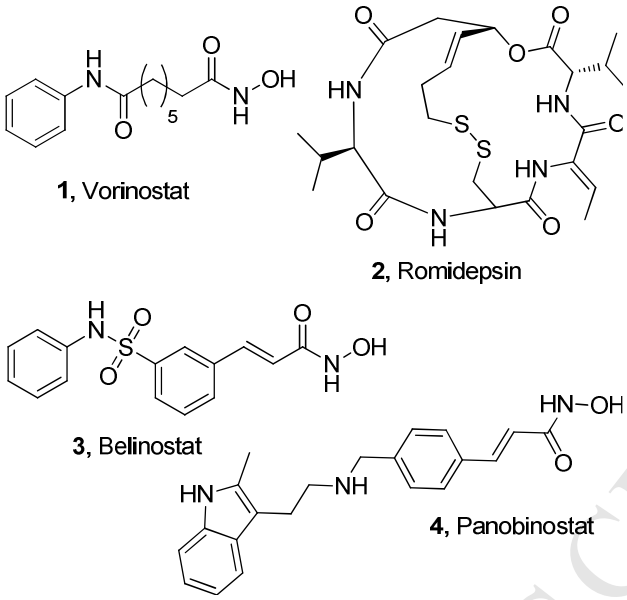

Figure 1. Approved histone deacetylase pan inhibitors **1**-**4**.

Notably, these drugs can show several side-effects since they are mainly pan-HDACi or targeting multiple HDAC isoforms [18]. Isoform-selective HDACi could display therapeutic benefits due to minimal toxicity and limited off-target effects [19]. Therefore, in the last years, isoform- or class-specific inhibition have caught the attention in HDACi research [20].

In our quest for the search of novel cancer therapeutics we decided to focus on HDAC6 isoform for a series of reasons. HDAC6 is crucially involved in several cellular processes including cell growth, survival and migration, but also in protein degradation and intracellular trafficking. Consequently, HDAC6 has been considered a potential target for the treatment of different types of malignancies inhibiting cancer cell migration and metastasis [21, 22]. HDAC6 displays a unique cytoplasmic localization [21, 23, 24], and it is active on a variety of non-histone protein substrates such as α-tubulin, peroxiredoxin, cortactin, and Hsp90 [25, 26]. On the contrary, among class I HDAC enzymes, HDAC 1, 2, and 3 are found primarily in the nucleus, whereas HDAC8 is found in both the nucleus and the cytoplasm. Additionally, the closest homolog of HDAC6, namely the cytosolic isozyme HDAC10, also belonging to class IIb HDACs, is not effective as lysine deacetylase. This is mainly due to the presence of a glutamate gatekeeper (replacing the lysine gatekeeper of HDAC6) and to a sterically constricted active site, which confer specificity for acetylpolyamine

substrates while disfavoring acetyllysine hydrolysis. Moreover, HDAC10 mainly promotes autophagy-mediated effects [27]. Class IIa HDAC enzymes (HDAC 4, 5, 7, and 9) are usually inefficient enzymes on standard substrates [28], although they lately displayed some utility in enhancing metabolic health in chronic diseases driven by physical inactivity [29].

In this scenario, selective HDAC6i have been developed as potential anticancer agents [23, 30-32]. However, design of structurally innovative and more selective inhibitors still represents an important task in drug discovery. In particular, although a variety of molecules advanced to clinic are considered selective HDAC6 inhibitors (eg. Ricolinostat and Citarinostat), their selectivity for HDAC6 isoform is only about 10-fold over HDAC1/2/3 isoforms (class I HDACs) [33]. On the contrary, preclinical candidates displaying higher HDAC6 selectivity (SI around 60), such as Tubastatin A, show severe liabilities due to its intrinsic toxicity to normal cells. As a continuation of our efforts in this field [34] the present study describes a thorough investigation of the active catalytic sites of HDAC1/6 and the development of a series of spiroindoline derivatives with preferred binding at HDAC6 isoform (Figure 2). Selectivity was investigated over HDAC1 (nuclear) and HDAC8 isoforms (nuclear/cytoplasmic) (Tables 1,2).

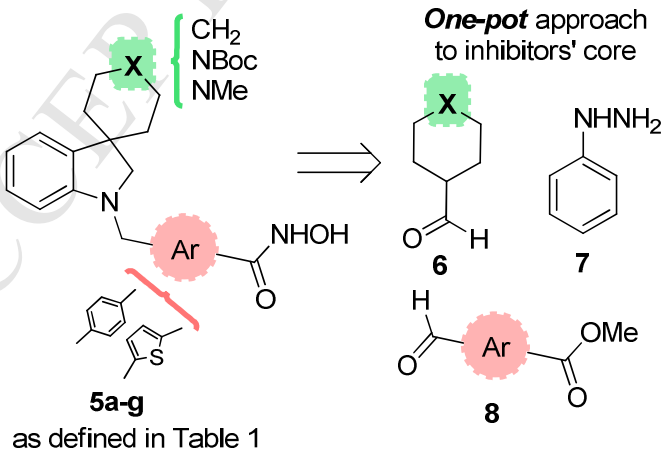

Figure 2. Retrosynthetic *one-pot* approach to the spiroindoline scaffold of title compounds **5a-g** (structures are defined in Table 1).

For the rational design of the new class of inhibitors, we took into account the general features for the HDACs inhibition, namely: i) a cap group interacting with the surface of the enzyme, ii) a linker and iii) a metal-binding group interacting with the catalytic zinc ion (zinc-binding group [ZBG] [35, 36]). In order to efficiently shape the newly conceived chemical entities to achieve selective HDAC6 inhibition, we envisaged the combination of a bulky spiroindoline cap group with a linker moiety containing an aromatic ring at appropriate distances from the ZBG (Figure 2). In particular, keeping in mind the notion that HDAC6, differently from other isoforms, can accommodate bulky rigid cap groups [37, 38], we aimed at building a cap group able to nicely accommodate in the HDAC binding site while also targeting a specific lipophilic pocket identified in HDAC6 and shaped by three residues, namely L749, F679 and F680. In the HDAC1 homolog the F679 is replaced by Y204 residue, and this could represent a further handhold for gaining potency and selectivity on HDAC6 over HDAC1 isoform. The spirocyclic indoline scaffold was preferred over an indoline substituted at C-3 by a flat aromatic system to favor interaction with the targeted lipophilic HDAC6 pocket. Beyond their increasing appearance in literature as useful medicinal chemistry and drug discovery templates [39-42], spiro-fused scaffolds may display a number of additional potential benefits. First, the insertion of a spiro-fused ring could allow the development of achiral molecules. Moreover, recent literature supports the use of spiro-compounds since the conformational restriction by spiro ring formation could potentially improve bioavailability and metabolic stability [43], reduce off-target activities and impart more favorable physical properties with respect to compounds containing many flat rings [44-48]. Spiro-ring fusion could also represent a useful method of increasing molecular complexity and may offer greater benefit than introduction of flat rings [46, 47]. Docking studies finally helped identifying a spiroindolyl cyclohexane and a spiroindolyl 4-piperidine templates as the preferential cap groups to be explored.

Regarding the linker and ZBG portions, our primary choice was a benzyl linker anchoring a *para*-hydroxamic functionality as the ZBG. This group already conferred strong HDAC6 selectivity to inhibitors such as TubA and its selection is also supported by recent studies highlighting a

monodentate interaction for phenylhydroxamate inhibitors as a signature of selectivity for HDAC6 versus class I HDACs [49, 50]. We also herein explored a thiophene-containing isosteric linker.

To generate the new molecules a straightforward multicomponent *one-pot* protocol was applied for the assembly of the desired *N*1-substituted spiroindoline core which allowed to rapidly perform a small series of focused structural variations at the spiro-fused piperidine terminal ring level in order to explore their effects on HDAC6 activity and selectivity (Figure 2). We then compared the outcome in HDAC1 and HDAC6 isoforms, in order to obtain unambiguous suggestions on general inhibitors' potency and selectivity, since HDAC1 is a representative member of a different deacetylase class displaying different phylogeny. Specifically, HDAC1 is representative of the HDAC enzymes with nuclear localization, while HDAC6 represents a cytoplasmic isoform. To further confirm the inhibitor selectivity profile in cell-based settings, the effects of selected compounds on histone H3 and α-tubulin acetylation levels (taken as markers of class I HDACs and HDAC6 inhibition, respectively) were determined. Moreover, the most promising inhibitors, in terms of both inhibitory profile and calculated drug-like properties, were evaluated for their effects on cell cycle and apoptosis in several tumor cell lines. The effects on the inhibition of cell migration and cell toxicity on mouse fibroblasts were also evaluated.

2. Chemistry

Compounds **5a-g** were synthesized exploiting a practical *one-pot* procedure for the simultaneous construction of the spiroindoline template bearing the linker moiety already in place. This chemical path was conceived for allowing the simple functionalization of all the portions of the indoline skeleton, with subsequent rapid analoging potential. In more details, the proposed scheme for the *one-pot* synthesis of indolines from arylhydrazines envisaged three key steps: i) a Fischer indole synthesis, starting from the suitable arylhydrazines and α,α-disubstituted aldehydes, providing the corresponding 3,3-disubstituted indolenines; b) a C=N bond reduction of the intermediate indolenines and c) reductive amination for *N*1 alkylation [51-53]. Accordingly, compound **5a** was

obtained following the procedure reported in Scheme 1. Cyclohexanecarboxaldehyde **6a** was reacted with phenyl hydrazine **7** in acetic acid at 80 °C. The indolenine formation was generally completed in 2-3 h and easily monitored by TLC and LC–MS analyses. Dilution with 1,2-dichloroethane was then followed by sequential addition of methyl 4-formylbenzoate **8a** and $NaBH(OAc)_3$. This procedure led to easily achieve the desired *N*1 functionalized spiroindoline template. Methyl ester functionality of compound **9** was then subjected to the final reaction with hydroxylamine and sodium hydroxide providing final compound **5a**.

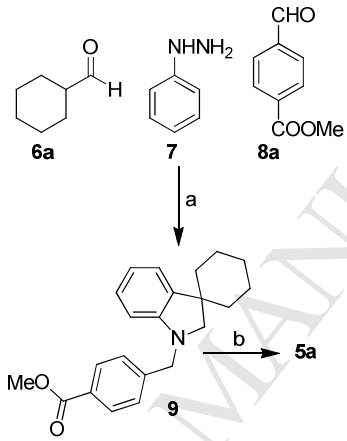

Scheme 1. Reagents and conditions: a) AcOH, 80 °C, 2 h then 0 °C, 1,2-DCE, $NaBH(OAc)_3$, 25 °C, 12 h; b) NH_2OH (50 wt. % in H_2O), NaOH, DCM/MeOH from 0 °C to 25 °C, 12 h.

The synthesis of compounds **5b-g** is described in Scheme 2. All the final compounds were obtained starting from two key intermediates, namely compounds **12** and **14**, deriving from the *one-pot* scaffold construction, thus demonstrating the versatility of the procedure.

For the synthesis of final compounds **5b-5e** the *one-pot* protocol previously described was employed starting from 1-Boc-piperidine-4-carboxaldehyde **6b**, in turn prepared from 1-Boc-4-piperidone **10**. This latter was homologated by means of a Wittig reaction. Treatment with (methoxymethyl)triphenylphosphonium chloride provided the enol ether **11** which was subsequently hydrolyzed with cerium(III) chloride in acetonitrile to the 1-Boc-piperidine-4-carboxaldehyde **6b** in good overall yield. For the preparation of the target compound **5b**, compound **6b** was subjected to a *one-pot* reaction with phenylhydrazine (**7**), methyl-4-formyl benzoate (**8a**),

and $NaBH(OAc)_3$ to obtain ester intermediate **12**. Reaction of this latter with hydroxylamine solution and sodium hydroxide led to final compound **5b**. Intermediate **12** was also Boc-deprotected and reacted with formaldehyde in the presence of $NaBH_3CN$ thus affording the corresponding *N*-methyl derivative, finally reacted with hydroxylamine, providing compound **5c**.

Intermediate **12** was also employed for the preparation of the two amide derivatives **5d,e**. After Boc deprotection, the resulting free amine was reacted with acetyl or pivaloyl chloride, respectively. Reaction with aqueous hydroxylamine and sodium hydroxide led to target compounds **5d,e**.

For the preparation of thiophene-based compounds **5f** and **5g**, aldehyde **8b** was obtained from bromoderivative **13** [34] which underwent reaction with 4-methylmorpholine *N*-oxide in acetonitrile. One pot reaction of **6b** and phenylhydrazine followed by addition of aldehyde **8b** led to the key intermediate methyl ester **14** employed for the synthesis of final compounds **5f,g**, following the procedure described for compound **5b,c**.

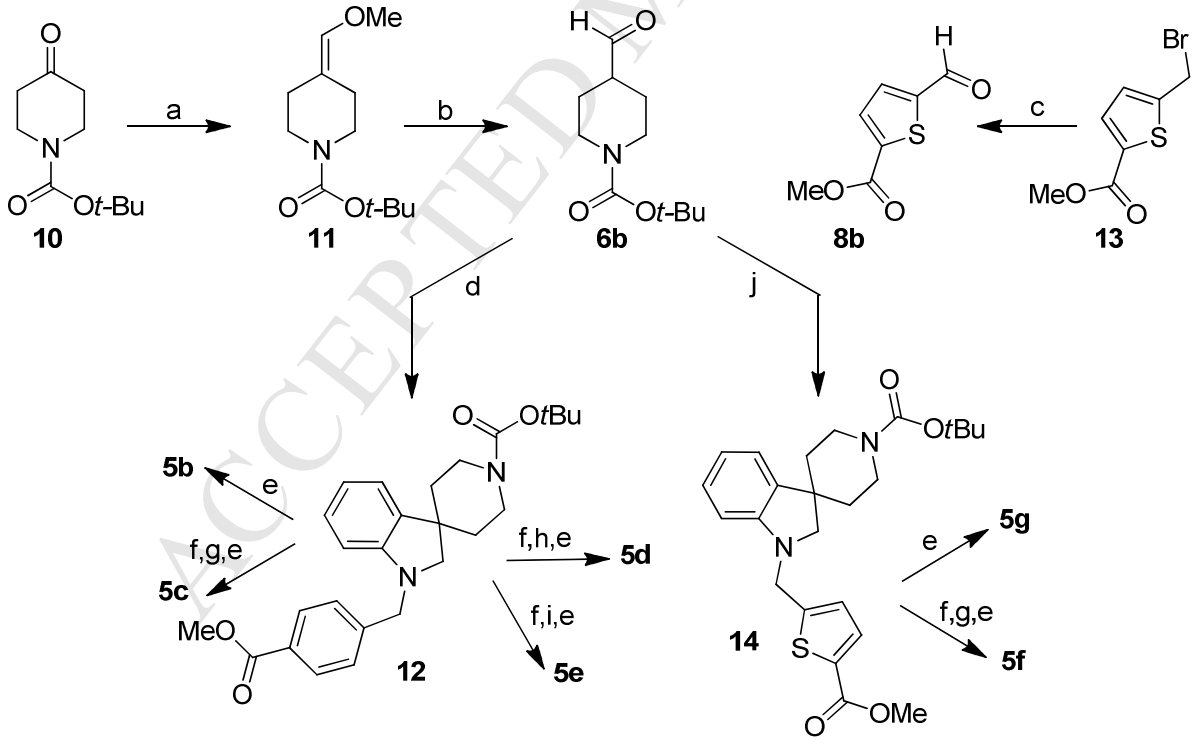

Scheme 2. Reagents and conditions: a) $(Ph)_3P(Cl)CH_2OMe$, NaHMDS, dry THF, 0 °C to 25 °C, 30 min; b) $CeCl_3{\cdot}7H_2O$, NaI, 40 °C, MeCN, 16 h; c) NMO, MeCN, 25 °C, 12 h; d) **7**, AcOH then **8a**, $NaBH(OAc)_3$, 1,2-DCE, 80 °C, 3 h, then 25 °C, 14 h; e) NH_2OH (50 wt. in % H_2O), NaOH, DCM/MeOH from 0 °C to 25 °C, 12 h; f) AcCl, MeOH, 25 °C, 18 min; g) CH_2O (37% aqueous

sol.), 1,2-DCE, 25 °C, 1 h, $NaBH_3CN$, 25 °C, 12 h; h) AcCl, TEA, DCM, 25 °C, 12 h; i) pivaloyl chloride, TEA, DCM, 25 °C, 12 h; j) **7**, AcOH then **8b**, $NaBH(OAc)_3$, 1,2-DCE, 80 °C, 3 h, then 25 °C, 14 h.

3. Results and discussion

3.1. Structure–activity relationship and molecular modelling studies

The inhibitory potency of the newly conceived compounds was evaluated *in vitro* against HDAC1 and HDAC6 enzymes, using a fluorescence-based activity assay [54]. The inhibition potency of compounds **5a-g** on HDAC1 and HDAC6 enzymes is reported in Table 1. Structure–activity relationship (SAR) analysis was performed coupling *in vitro* data with computational studies based on molecular docking calculations using Glide employing Standard Precision (SP) as scoring function. The calculation outcome provides a general trend that highlights the preferred binding of spiroindoline compounds at HDAC6 isoform.

Table 1. Inhibitory activity as IC_{50} (nM) ± standard error and Glide docking score (standard precision, SP; kcal/mol) against HDAC1 and HDAC6 enzymes and HDAC1/HDAC6 selectivity ratio.

Cpd	Structure	IC_{50} HDAC1 (μM)	IC_{50} HDAC6 (nM)	HDAC1/ HDAC6	Glide SP HDAC1 (kcal/mol)	Glide SP HDAC6 (kcal/mol)
5a	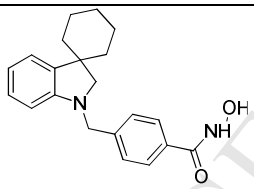	6.79 ± 1.02	40.9 ± 6.9	166	-8.367	-9.967
5b	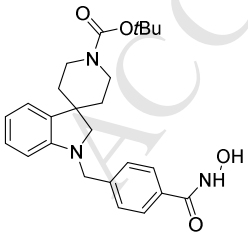	4.00 ± 0.78	41.9 ± 7.9	95	-8.701	-10.194
5c	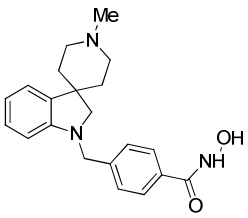	11.71 ± 0.71	203.8 ± 28.4	57	-8.550	-9.435

5d	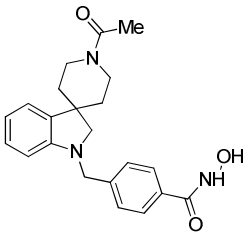	7.29 ± 0.79	62.5 ± 14.5	116	-8.707	-9.838
5e	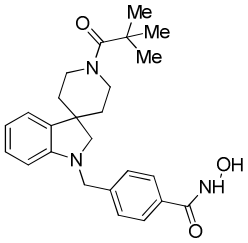	4.47 ± 0.50	60.1 ± 7.9	74	-8.373	-9.539
5f	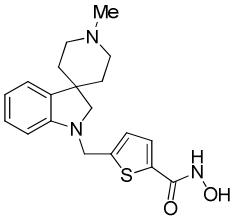	11.44 ± 3.29	1780 ± 350	6	-8.004	-9.124
5g	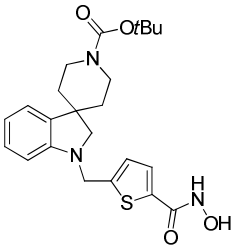	10.87 ± 5.67	718.6 ± 73.5	15	-8.138	-9.013
Tubastatin A	-	1.91 ± 0.42	30.4 ± 2.1	63	-8.277	-9.878

Using docking calculations, we observed a conserved trend in the binding modes of this series of developed compounds into HDAC1 and 6 isoforms' binding sites. In particular, **5b** could be able to form a metal coordination bond into both isoforms (Figure 3), although we noticed a different pattern of interaction. Compound **5b** into HDAC1 binding site is able to form only one H-bond with the backbone of G149 and limited hydrophobic contacts with F150 (especially π-π stacking interaction) and L271. The bulky piperidyl-*N*-*tert*-butyl carbamate group appears to be largely solvent exposed with few hydrophobic interactions with Y204. This binding mode could support its micromolar inhibitory potency against HDAC1. On the contrary, the binding mode of compound **5b** into HDAC6 shows an increased number of contacts. In detail, besides the potential metal coordination bond with the Zn^{2+} ion, **5b** forms a series of H-bonds with H610, G619 (backbone),

and Y782. The benzene ring of the linker moiety is able to establish a double π-π stacking with F620 and F680. Gratifyingly, in full agreement to our design strategy, the spiropiperidyl moiety nicely fits within the targeted hydrophobic pocket (L749, F679 and F680). Interestingly, the optimum accommodation of the spiro-fused portion also allowed the terminal *t*-butylcarbamate functionality to establish strong hydrophobic interactions with the side chains of T678 and F679 (Figure 3), contrarily to what observed for HDAC1 isoform. The major number of established contacts is in agreement with the registered higher inhibitory potency of compound **5b** against HDAC6 vs HDAC1 with 100-fold selectivity (IC_{50} HDAC1 = 4.00 μM; IC_{50} HDAC6 = 41.9 nM, Table 1).

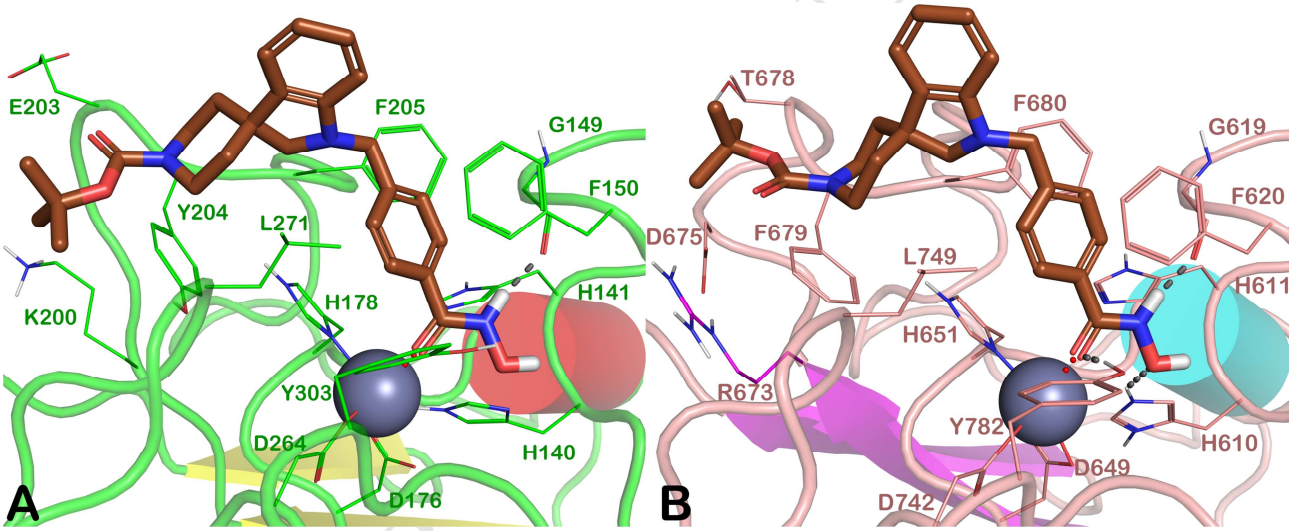

Figure 3. Docked poses of **5b** into HDAC1 (panel A) and HDAC6 (panel B). Compound **5b** is represented as sticks while the residues in the active sites are represented as line and the protein is represented as cartoon. Zn^{2+} is represented as a gray sphere. H-bonds are represented as black dotted lines, while red and blue dotted lines represent the metal coordination bonds.

Similarly to **5b**, **5a** showed a comparable behavior into HDAC1 and HDAC6 enzymes (Figure S1). The absence of the *t*-butylcarbamate functionality allows the indoline moiety to improve the hydrophobic contacts with F150 (HDAC1) and F620 (HDAC6), maintaining the other interactions already described for **5b**. Accordingly, the experimental IC_{50}s against HDAC1/6 are comparable to

those found for **5b**. The introduction of an *N*-Me group replacing the *t*-butylcarbamate led to compound **5c** displaying a slight decrease of affinity towards both HDAC isoforms with an inhibitory potency of IC_{50} HDAC1 = 11.71 μM; IC_{50} HDAC6 = 203.8 nM. Although the docking outputs depicted in Figure S2 are very similar to those found for **5a**, the introduction of a protonatable group such as *N*-Me on the spiro-fused terminal ring is not well tolerated by both enzymes. This event could be due to the presence, in both binding sites of the two isoforms, of positively charged amino-acids such as K200 in HDAC1 and R673 in HDAC6 and to the not favorable desolvation energy for this compound. The insertion on the terminal spiro-fused ring of an *N*-acetyl or a *N*-trimethylacetyl group led to compounds **5d** and **5e**, respectively. These substitutions are well tolerated from HDAC6 and allow keeping significant selectivity over HDAC1. The docking outputs of **5d** (Figure S3) and **5e** (Figure S4) into both enzyme subtypes are comparable to those obtained for **5b**, as supported by experimentally determined inhibitory potencies (Table 1). The replacement of the benzene ring in compound **5c** with thiophene led to compound **5f**. In this latter, the presence of a protonatable group (*N*-Me) combined with a smaller aromatic moiety in the linker caused a dramatic decrease in both affinity and isoform selectivity. Beyond the already discussed unfavorable effects due to the *N*-Me insertion, we registered also a reduction of π-π stacking in both enzymes. As reported in Figure 4, **5f** was not able to establish a double π-π stacking into HDAC6 but is able to stack only with F620. Regarding HDAC1 a different orientation of the thiophene was encountered with respect to the benzene ring of the previously described compounds, resulting in an unfavorable conformational energy of the poses as detected by docking calculation, and in the lower inhibitory potency against HDAC1 and HDAC6 (IC_{50} HDAC1 = 11.44 μM; IC_{50} HDAC6 = 1780 nM).

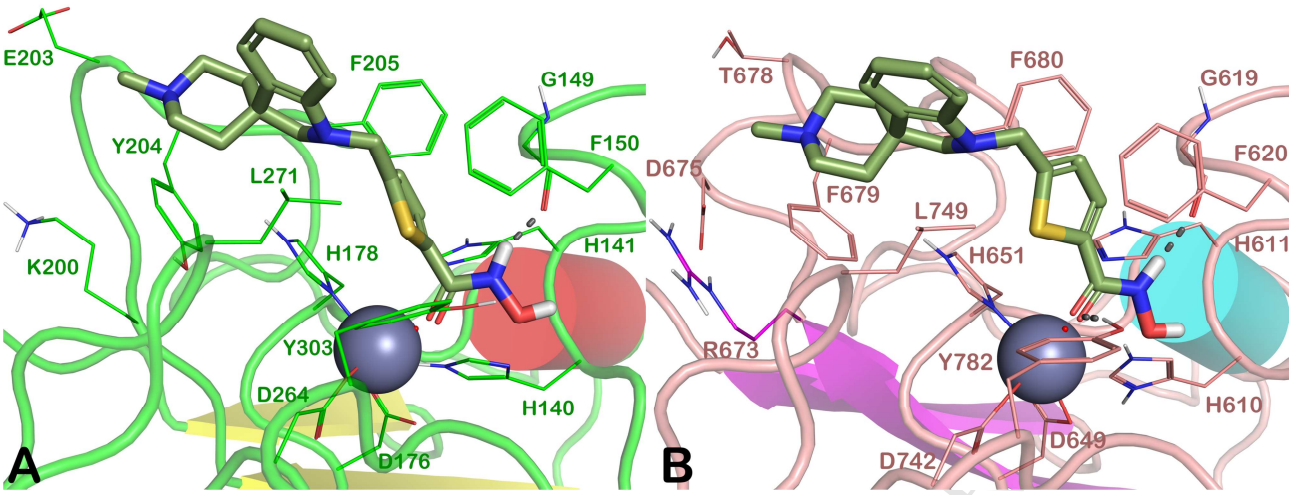

Figure 4. Docked poses of **5f** into HDAC1 (panel A) and HDAC6 (panel B). Compound **5f** is represented as sticks while the residues in the active sites are represented as line and the protein is represented as cartoon. Zn^{2+} is represented by a gray sphere. H-bonds are represented as black dotted lines, while red and blue dotted lines represent the metal coordination bonds.

The replacement of the basic tertiary amine of **5f** by a *t*-butylcarbamate led to compound **5g**. As expected, this compound showed a slight improvement in inhibitory potency against HDAC6, although lower than its benzene counterpart **5b**. **5g** (Figure S5) demonstrates a similarity to **5f** in the binding mode. These findings support the *in vitro* and computational data reported in Table 1.

As a further indication on the selectivity of compounds, we also assessed the potency of three representative inhibitors (compounds **5a,b,g**, Table 2) on HDAC8 isoform, which is unique in class I HDACs, since it recognizes both histone and non-histone substrates. Moreover, HDAC8 is ubiquitously expressed and can localize to either the nucleus (primary site) or the cytoplasm [55]. Compound **5b** displayed the lower activity of HDAC8 (IC_{50} = 1.602 µM), thus confirming its very selective interaction with HDAC6 enzyme. Compounds **5a** and **5g** displayed moderate selectivity over HDAC8 isoform.

Table 2. Inhibitory activity as IC_{50} (µM) ± standard error against HDAC8 enzyme.

Cpd	**5a**	**5b**	**5g**	**TubA**
IC_{50} (µM)	0.253 ± 0.018	1.602 ± 0.166	1.344 ± 0.157	0.695

We also predicted the *in silico* drug-like features of the novel chemical entities in order to support the selection process for the compounds to be advanced in cell-based studies. In particular, we used different tools such as QikProp, FaFDrugs [56] and an in-house 3D-QSAR model for predicting *h*ERG K^+ channel affinity (3D-chERGi) [57]. The outputs of these calculations are reported in Table S1. Additionally, the compounds were evaluated for their potential ability to behave as Pan Assay Interference Compounds (PAINS). This calculation was performed by means of FAFDrugs. Remarkably, the results showed that none of the compounds contain sub-structural features that would label them as "frequent hitters" in high-throughput screens. The molecular properties of the compounds showed satisfactory results, displaying suitable predicted aqueous solubility (cLogS), and cLogP. The membrane permeability was considered acceptable as well as the predicted human oral adsorption. No violation of Lipinski's rules was found. Compounds **5a**, **5b**, **5d**, **5e** and **5g** were predicted to possess limited affinity for the *h*ERG K^+ channel, while **5c** and **5f** could potentially interact with it. Although the molecular properties of the compounds showed satisfactory results, compounds **5d** and **5f** were not furthered in cell-based assays, since globally possessing the less satisfactory drug-like profile.

4. Cellular studies

Based on *in vitro* determined HDAC affinity and HDAC6 isoform selectivity and on the calculated drug-like properties, a selection of four derivatives (**5a-c** and **5e**) were engaged in Western blotting analyses to evaluate the levels of acetylation of α-tubulin (AcTub) and of histone H3 in lysines 9 and 14 ($H3K_{9,14}ac$). Acute promyelocytic leukemia NB4 and glioblastoma U87 cell lines were stimulated with compounds **5a**, **5b**, **5c** at 1 and 5 µM for 30 hours, in comparison with Vorinostat (**1**, SAHA) and Tubastatin, used as positive controls (Figure 5A). In NB4 cells all the assayed compounds were able to increase the levels of AcTub at 5 µM, while only compounds **5a** and **5c** increased the levels of $H3K_{9,14}ac$ (Figure 5A, top). Compound **5b**, in particular, showed a HDAC6-

selective mode of action. In U87 cell line all compounds were able to affect the levels of histone acetylation but **5c** and **5a** induced a dose-dependent increase of AcTub (Figure 5A, bottom).

In addition, due to the superior profile of **5b** in terms of activity and selectivity, its outcome on histone and tubulin acetylation was evaluated in neuroblastoma SH-SY5Y cells (Figure 5B). Interestingly, **5b** induced a dose-dependent increase in acetylation levels of tubulin, but not of histone H3, compared to the positive controls. The levels of tubulin acetylation were also higher than those measured with Tubastatin A (a selective HDAC6 inhibitor) and SAHA (**1**, a pan-HDAC inhibitor). All these data highlight compound **5b** as an extremely selective HDAC6 inhibitor also in cell-based settings.

Finally, in order to directly compare their HDAC6 selectivity in cell-based assays, compounds **5b** and **5e** (one of the best performing compounds in terms of calculated physico-chemical properties) were tested in NB4 and U87 cell lines (Figure 5C) by Western blotting analyses. Both compounds showed improved selectivity for HDAC6 compared to **1**.

ACCEPTED MANUSCRIPT

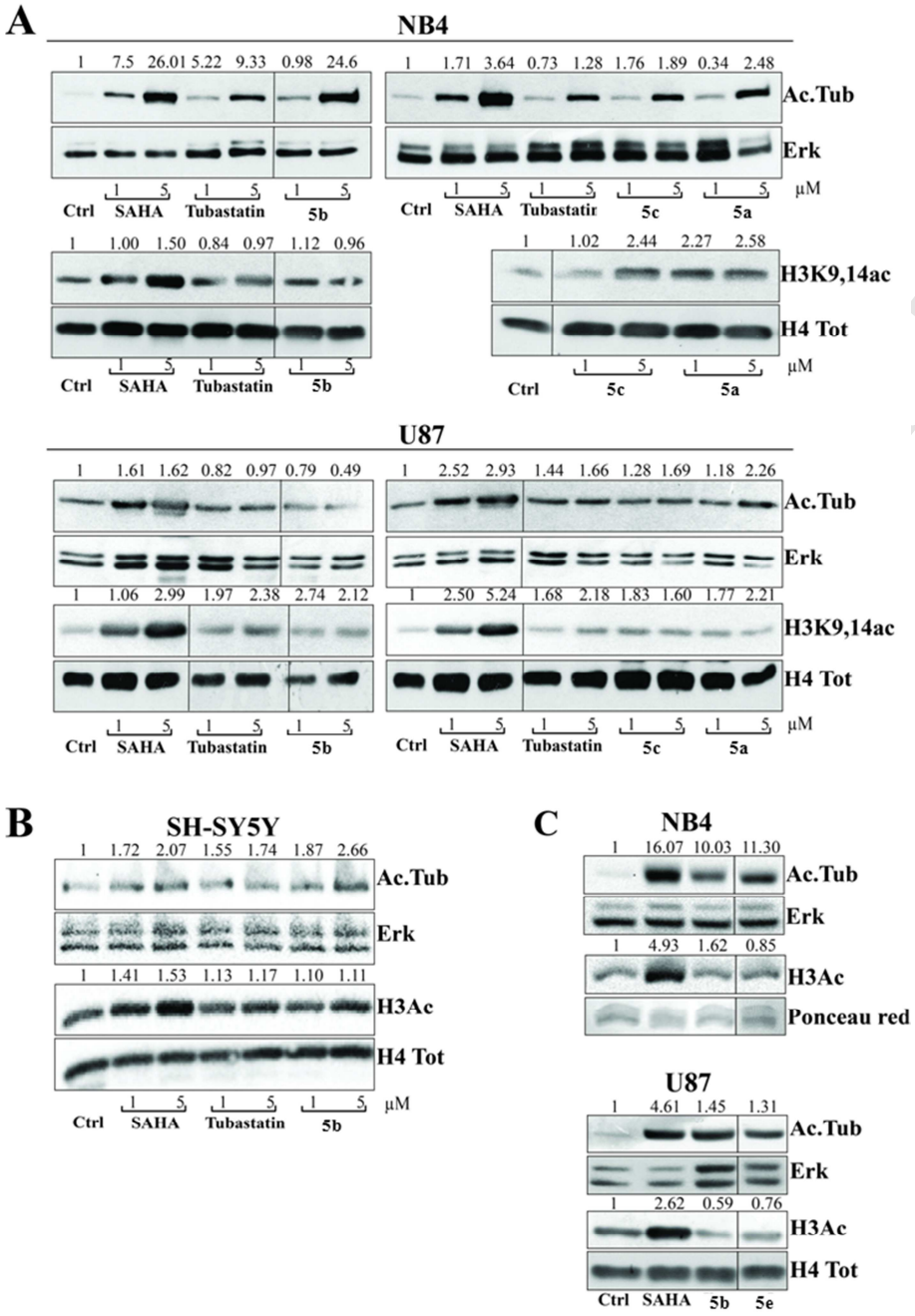

Figure 5. Western blot analyses of acetylation levels of the α-tubulin (AcTub) and histone H3 in lysines 9 and 14 ($H3K_{9,14}ac$) after 30 hours of the indicated treatments in NB4 and U87 (A), SH-SY5Y (B), and NB4 and U87 (C) cell lines. ERKs, total (Tot) histone H4 and Ponceau Red signals were used as loading controls.

By FACS analysis in NB4 cells, compound **5e**, when tested at 5 μM, induced a G1-phase arrest of cell cycle progression, similar to **1** (Figure 6A). Notably, both **5b** and **5e** were able to induce cell death, as revealed by the percentage of DNA fragmentation. Compound **5b**, at 5 μM, displayed a

higher cytotoxic activity than **1** and **5e** (Figure 6B). Collectively, these data suggest a promising antitumor activity for these two compounds.

Moreover, since HDAC6 displays unique features with respect to other HDAC isoforms, being mainly devoted to the deacetylation of non-histone proteins strongly involved in cell-cell interaction, motility and apoptosis, selective HDAC6 inhibitors display crucial importance for investigating and dissecting the specific roles of different HDAC enzymes in cancer. In particular, due to the role of HDAC6 in the regulation of microtubule- and actin-dependent cell mobility [58], inhibitor **5b** was evaluated in real-time migration assay (see Experimental Section for description). Interestingly, **5b** significantly inhibited migration of SH-SY5Y neuroblastoma cells (Figure 6C). The migration inhibitory effect of **5b** evaluated by slope analysis showed a strong decrease of migration rate after about 4 days of treatment, suggesting a strong anti-invasion effect of the drug. These data strongly imply wide-ranging anti-proliferative, anti-invasiveness and apoptotic effects of **5b** in low micromolar range.

ACCEPTED MANUSCRIPT

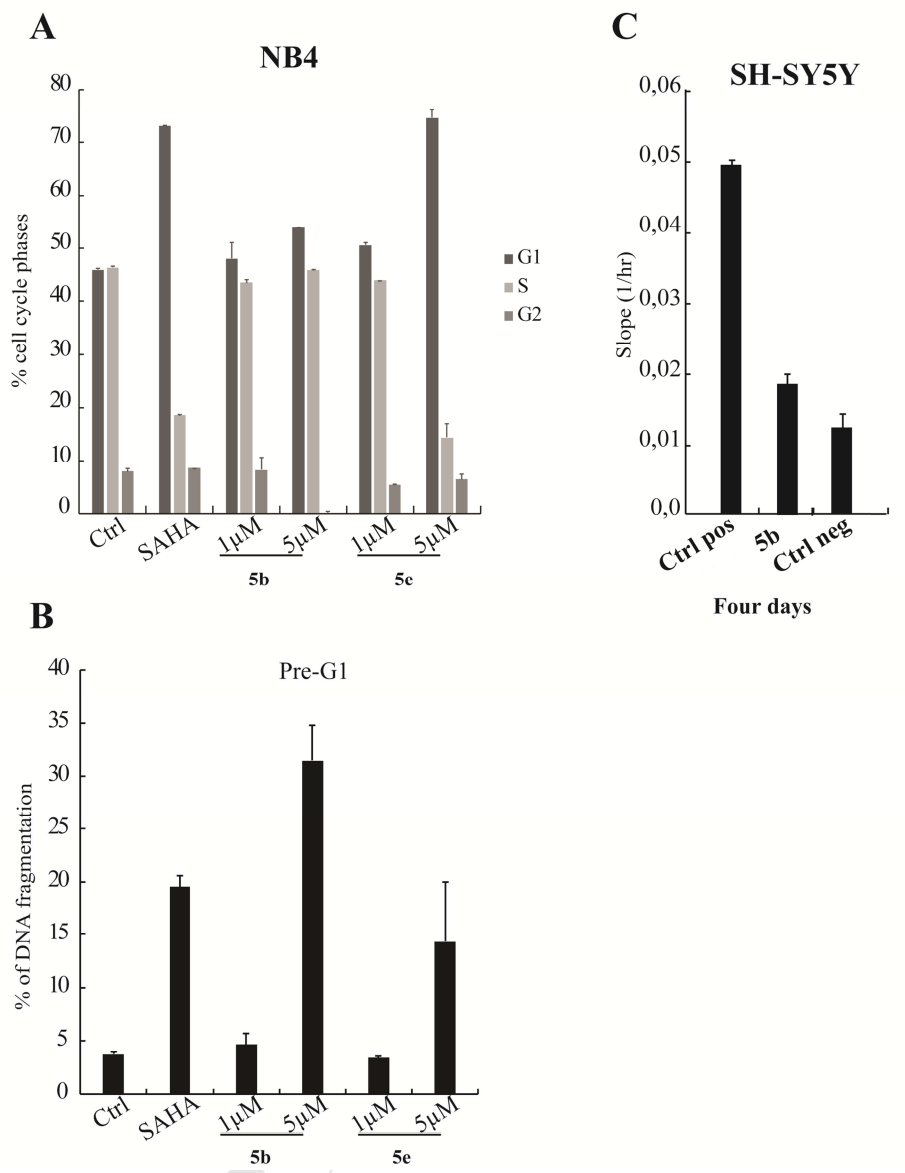

Figure 6. (A, B) Cell cycle and pre-G1 analyses in NB4 cell lines treated for 30 h with indicated compounds. (C) Migration inhibitory action of **5b** measured in SH-SY5Y as Slope (1/h) by xCELLigence Real-Time Cell Analyzer (RTCA) DP instrument (Roche).

To further characterize the profile of compound **5b**, we also performed a cytotoxicity assay to establish the effect on mouse fibroblasts NIH3T3 cells. Cell viability was measured by the Neutral Red Uptake test and data normalized as % control. We observed a TC_{50} on NIH3T3 cells of 23 μM, thus indicating a low toxicity for normal cells and a potentially favourable safety margin.

5. Conclusion

We herein described a series of spiroindoline derivatives rationally designed to preferentially bind the HDAC6 isoform. This goal was reached by combining medicinal chemistry and biological efforts. Our focused design strategy ultimately led to compounds displaying up to 170-fold selectivity for HDAC6 over HDAC1 isoform. A practical *one-pot* synthetic path was developed to build a focused set of *N*1-substituted spiroindoline cores. The versatility of the strategy will allow future scaffold manipulation and rapid analoging. The developed inhibitors were submitted to enzyme assays and the best performing compounds were engaged in cell-based assays to establish selectivity on cells and anticancer potential. Their influence on tubulin and histone acetylation status was evaluated to further confirm their HDAC6 selectivity. Moreover, the best performing derivatives were assessed for their effects on cell cycle and apoptosis, showing a promising antitumor potential in tumor cell lines. A selected derivative, **5b**, characterized by a piperidyl-*N*-*tert*-butyl carbamate, was further investigated revealing a significant potential in inhibiting tumor cells migration. Additionally, this compound did not display toxicity in NIH3T3 mouse fibroblasts and was found to possess satisfactory predicted drug-like properties. Regarding the *tert*-butyl carbamate moiety of our hit **5b**, it is interesting to mention that carbamates are present in many approved drugs [59] and in particular, *tert*-butyl carbamates of piperidine derivatives have been reported to accomplish drug-like properties [60]. Taken together, these data highlight a promising antitumor potential for the developed compounds. Further studies and compound optimization are ongoing in our laboratories.

6. Experimental Section

6.1. Chemistry

Unless otherwise specified, materials were purchased from commercial suppliers and used without further purification. Reaction progress was monitored by TLC using silica gel 60 F254 (0.040–0.063 mm) with detection by UV. Silica gel 60 (0.040–0.063 mm) was used for column chromatography. 1H NMR and 13C NMR spectra were recorded on a Varian 300 MHz spectrometer or a Bruker 400 MHz spectrometer by using the residual signal of the deuterated

solvent as internal standard. Splitting patterns are described as singlet (s), doublet (d), triplet (t), quartet (q) and broad (br); the values of chemical shifts (δ) are given in ppm and coupling constants (*J*) in Hertz (Hz). Microwave reactions were performed by a CEM Discovery apparatus. ESIMS spectra were performed by an Agilent 1100 Series LC/MSD spectrometer. The yields are referred to purified products and are not optimized. All moisture-sensitive reactions were performed under argon atmosphere using oven-dried glassware and anhydrous solvents. Experimental procedures and characterization for the novel compounds are reported in Supplementary Material. Final compounds were analyzed by combustion analysis (CHN) to confirm purity > 95% (Table S2).

6.2. Computational details

All calculations were performed using two workstations (Intel Core i5–2400 CPU @3.10 GHz Quad; Intel Core i5–2500 CPU @ 3.30 GHz Quad) with Ubuntu 17.04 OS, running Maestro 10.1 (Schrödinger, LLC, NY, USA, 2015). Figures depicting docking outputs were prepared using PyMOL (The PyMOL Molecular Graphics System, v1.8.4.0, Schrödinger LLC, New York, 2015).

6.2.1. Molecular Docking simulations

6.2.1.1. Proteins and ligands preparation

Crystal structures of human HDAC1 (PDB ID 4BKX [61]) and HDAC6 (PDB ID 5EDU [37]) were taken from PDB and submitted to Protein Preparation Wizard (PPW) protocol implemented in Maestro suite 2015 in order to obtain suitable protein structures for molecular docking calculations as previously reported [62-64]. Ligands, water molecules and compounds used in the crystallization process were removed maintaining the Zn^{2+} ion [34]. By following PPW protocol we performed a series of computational steps to: (1) generate metal binding state for the enzymes (2) add hydrogens, (3) optimize the orientation of hydroxyl groups, Asn, and Gln, and the protonation state of His, and (4) perform a constrained minimization refinement with the *impref* utility. The refined proteins were used in molecular docking calculation as reported in the next paragraph.

The 3D structure of ligands reported in Table 1 and those of reference compounds (Trichostatin A, Tubastatin A and **1**) were built in Maestro 10.1 (Schrödinger, LLC, New York, NY, 2015).

MacroModel software was used for the energy minimizations employing the OPLS-2005 force field. The solvent effects were simulated using the analytical Generalized-Born/Surface-Area (GB/SA) model [65], and no cutoff for nonbonded interactions was selected. Polak-Ribiere conjugate gradient (PRCG) method with 1000 maximum iterations and 0.001 gradient convergence threshold was employed. All compounds reported in this paper were treated by LigPrep application (LigPrep version 3.3, Schrödinger, LLC, New York, NY, 2015) in order to generate the most probable ionization state at cellular pH (7.4 ± 0.2) as reported by us [66, 67]. Moreover, according to the evidences reported in literature [68-73], we used a neutral hydroxamic acid moiety of the spiroindoline compounds, since the hydroxamic acid proton should not be transferred in HDAC isoforms containing histidines in the binding site close to the reactive metal center, as in the case of HDAC1 and HDAC6.

6.2.1.2. Molecular Docking

Glide software (Glide, version 6.6, Schrödinger, LLC, New York, NY, 2015) has been employed to perform the docking studies presented in this paper, using the ligands and proteins prepared as above-mentioned, applying Glide standard precision (SP) scoring function. Energy grids were prepared using default value of protein atom scaling factor (1.0 Å) within a cubic box centered on the zinc ion which roughly represents the center of the active sites [34]. After grid generation with the introduction of metal constrains, the ligands were docked into the enzymes. The number of poses entered to post-docking minimization was set to 50. Glide SP score was evaluated. In order to assess the validity of docking protocol, **1** and Trichostatin A were used as reference compounds for a re-docking procedure. The docking results revealed a similar accommodation for the above mentioned reference compounds with respect to the previously published results (data not shown) [37, 74].

6.2.2. Molecular properties prediction

Molecular properties were evaluated by means of QikProp (QikProp, version 4.3, Schrödinger, LLC, New York, NY, 2015), while the assessment for potential Pan Assay Interference Compounds

(PAINS) within the set of selected molecules was conducted by means of FAFDrugs4.0 (http://fafdrugs4.mti.univ-paris-diderot.fr/ access date December 2017). The evaluation of *h*ERG K^+ channel affinity was performed using our inclusive in-house 3D-QSAR model (3D-chERGi) [57].

6.3. *In vitro* testing of HDAC1, HDAC6 and HDAC8

OptiPlate-96 black microplates (Perkin–Elmer) were employed with an assay volume of 60 μL. Human recombinant HDAC1 (BPS Bioscience, Catalog #: 50051) or human recombinant HDAC6 (BPS Bioscience, Catalog #: 50006) were diluted in incubation buffer (50 mM Tris-HCl, pH 8.0, 137 mM NaCl, 2.7 mM KCl, 1 mM $MgCl_2$ and 1 mg/ml BSA). A total of 52 μL of this dilution were incubated with 3 μL of different concentrations of inhibitors in DMSO and 5 μL of the fluorogenic substrate ZMAL (Z-(Ac)Lys-AMC) [75, 76] (126 μM) at 37 °C. After 90 min incubation time, 60 μL of the stop solution (33 μM Trichostatin A and 6 mg/mL trypsin in trypsin buffer [Tris-HCl 50 mM, pH 8.0, NaCl 100 mM]), were added. After a following incubation at 37 °C for 30 min, the fluorescence was measured on a BMG LABTECH POLARstar OPTIMA plate reader (BMG Labtechnologies, Germany) with an excitation wavelength of 390 nm and an emission wavelength of 460 nm [54, 76].

Recombinant hHDAC8 was produced as described before [77]. The HDAC8 activity assay was performed using a commercial HDAC8 fluorimetric drug discovery kit [Fluor de Lys(R)-HDAC8, BMLKI178] according to the manufacturer's instructions as described earlier [78]. The enzyme was incubated for 90 min at 37 °C, with a substrate concentration of 50 μM and increasing concentrations of inhibitors. Measurement was performed as described for HDAC1/6.

6.4. Biological section

6.4.1. Cell lines

Glioblastoma, U87 (ATCC) and neuroblastoma cell lines, SH-SY5Y (ATCC) were propagated in DMEM medium (Euroclone, Milan, Italy) with 10% fetal bovine serum (FBS) (Euroclone), 2 mM L-glutamine (Euroclone) and antibiotics (100 U/ml penicillin, 100 l g/ml streptomycin) (Euroclone). Human Acute Promyelocytic Leukemia, NB4 cell line, was propagated in RPMI 1640

medium with 10% FBS (Euroclone), 100 U/mL penicillin-streptomycin (Euroclone) and 2 mM L-glutamine (Euroclone). Cells were stimulated with drugs for 30 h at 1µM and 5µM.

6.4.2. Western blot analysis

To quantify the acetylation levels, we performed the total protein and the histone extraction by evaluation respectively of Ac-tubulin and histone $H3K_{9,14}ac$ or H3Ac.

6.4.2.1. Total protein extraction

The cells were harvested, washed with PBS (Euroclone), and lysed for 15 min at 4 °C in lysis extraction buffer with protease and phosphatase inhibitors: 50 mM Tris-HCl pH 8.0, 150 mM NaCl, 1% NP40, 10 mM sodium fluoride, 0.1 mM sodium orthovanadate, 40 mg/mL phenylmethylsulfonyl fluoride (PMSF), 20 g/mL aprotinin, 20 mg/ml leupeptin, 2 mg/mL antipain, 10 mM p-nitrophenyl phosphate, 10 mg/mL pepstatin A and 20 nM okadaic acid. Cells were then centrifuged at 13000 rpm for 30 minutes at 4 °C, and protein content of supernatant was used to determine the protein concentration by colorimetric assay (Biorad, Italy). Cell extracts were diluted 1:1 in sample buffer 2X Laemmli (0.217 M Tris-HCl pH 8.0, 52.17% SDS, 17.4% glycerol, 0.026% bromo-phenol blue, 8.7% beta-mercapto-ethanol), and then boiled for 3 minutes. Equal amounts of protein (50 µg) were run and separated by SDS-PAGE gel (acrylamide gel). Primary antibodies used were acetyl-tubulin (Sigma) and anti-ERKs antibody (Santa Cruz Biotechnology) was used for normalization.

6.4.2.2. Histone extraction

Cells were harvested and washed twice with cold 1X PBS and lysed in Triton extraction buffer (TEB; PBS containing 0.5% Triton X 100 (v/v), 2 mM PMSF, 0.02% (w/v) NaN_3) at a cell density of 107 cells/mL for 10 min on ice, with gentle stirring. After centrifugation (2,000 rpm at 4 °C for 10 min), the supernatant was removed, and the pellet was washed in half the volume of TEB and centrifuged as before. The pellet was suspended in 0.2 N HCl at a cell density of 4 × 107 cells/mL overnight at 4 °C on a rolling table. The samples were then centrifuged at 2,000 rpm for 10 min at 4 °C, the supernatant was removed, and the protein content was determined using a Bradford assay

(Bio-Rad, CA, USA). For the detection of histone H3 acetylation, we used H3Ac (Abcam) or $H3K_{9,14}ac$ (diagenode). Histone H4 (Abcam) antibodies and Pounceau Red (Sigma) were used to normalize for equal loading. Semi-quantitative analysis was performed using Fiji software [79].

6.4.3. Cell cycle analysis

Cells after stimulation were collected. The cells were then centrifuged (1,200 rpm for 5 min) and suspended in 500 µL a solution containing 1 × PBS, 0.1% sodium citrate, 0.1% NP40 and 50 mg/mL propidium iodide (Sigma Aldrich). The samples were incubated for 30 min at room temperature in the dark. Cell cycle was evaluated by FACS-Calibur (Becton Dickinson) and analyzed with ModFit v3 software (Verity Software House). Apoptosis was measured as Pre-G1 analyzed by FACS with Cell Quest software (BD Biosciences) [80]. Experiments were performed in duplicate.

6.4.4. Cell migration assay

Cell migration was analysed in real time without exogenous labels using the Roche xCELLigence Real-Time Cell Analyzer (RTCA) DP instrument. The RTCA DP instrument uses the CIM (cellular invasion/migration)-Plate 16 featuring microelectronic sensors integrated into the underside of the micro-porous polyethylene terephthalate (PET) membrane of a Boyden-like chamber. In response to the chemo-attractant (FBS) the cells migrate from the upper chamber through the membrane into the bottom chamber thus contacting and adhering to the electronic sensors on the underside of the membrane, resulting in an increase in impedance that is proportional to increasing numbers of migrated cells on the underside of the membrane. CI values reflecting impedance changes are registered by the RTCA DP instrument. The membrane was pre-incubated for one hour in the CO_2 5% at 37 °C with serum-free medium before obtaining a background measurement. After the cell index measure, the SH-SY5Y cells were added to the top chamber CIM-Plate at the desired concentration. The migration was monitored every two minutes for several hours. The cells were analysed in absence or presence of 10% FBS in the bottom chamber. Cell migration was detected

by real-time monitoring and low and high seeding densities were quantitatively monitored and reflected by the CI values [81].

Acknowledgement

The authors thank COST Action CM1406. This study was supported by grants from MIUR (Rome, grants PRIN-2010M2JARJ to G. Campiani) and by the Deutsche Forschungsgemeinschaft (DFG, Ju 295/13-1) to J. S. and M. J. T. B. S. and C. R. are supported by institutional funds from the Centre National de la Recherche Scientifique (CNRS), the Institut National de la Santé et de la Recherche Médicale (INSERM) and the Université de Strasbourg.

Supplementary data

Supplementary data associated to this article can be found at….

References

[1] A. Villagra, E.M. Sotomayor, E. Seto, Histone deacetylases and the immunological network: implications in cancer and inflammation, Oncogene, 29 (2010) 157-173.
[2] S.Y. Roth, C.D. Allis, Histone acetylation and chromatin assembly: a single escort, multiple dances?, Cell, 87 (1996) 5-8.
[3] S.E. Polo, G. Almouzni, Histone metabolic pathways and chromatin assembly factors as proliferation markers, Cancer Lett., 220 (2005) 1-9.
[4] J.H. Tang, H.D. Yan, S.G. Zhuang, Histone deacetylases as targets for treatment of multiple diseases, Clin. Sci., 124 (2013) 651-662.
[5] M. Haberland, R.L. Montgomery, E.N. Olson, The many roles of histone deacetylases in development and physiology: implications for disease and therapy, Nat. Rev. Genet., 10 (2009) 32-42.
[6] H.J. Kim, S.C. Bae, Histone deacetylase inhibitors: molecular mechanisms of action and clinical trials as anti-cancer drugs, Am. J. Transl. Res., 3 (2011) 166-179.
[7] M. Duvic, R. Talpur, X. Ni, C.L. Zhang, P. Hazarika, C. Kelly, J.H. Chiao, J.F. Reilly, J.L. Ricker, V.M. Richon, S.R. Frankel, Phase 2 trial of oral vorinostat (suberoylanilide hydroxamic acid, SAHA) for refractory cutaneous T-cell lymphoma, (CTCL), Blood, 109 (2007) 31-39.
[8] K.M. VanderMolen, W. McCulloch, C.J. Pearce, N.H. Oberlies, Romidepsin (Istodax, NSC 630176, FR901228, FK228, depsipeptide): a natural product recently approved for cutaneous T-cell lymphoma, J. Antibiot., 64 (2011) 525-531.
[9] H.Z. Lee, V.E. Kwitkowski, P.L. Del Valle, M.S. Ricci, H. Saber, B.A. Habtemariam, J. Bullock, E. Bloomquist, Y. Li Shen, X.H. Chen, J. Brown, N. Mehrotra, S. Dorff, R. Charlab, R.C. Kane, E. Kaminskas, R. Justice, A.T. Farrell, R. Pazdur, FDA Approval: Belinostat for the Treatment of Patients with Relapsed or Refractory Peripheral T-cell Lymphoma, Clin. Cancer Res., 21 (2015) 2666-2670.
[10] K.P. Garnock-Jones, Panobinostat: first global approval, Drugs, 75 (2015) 695-704.

[11] G. Garcia-Manero, S. Assouline, J. Cortes, Z. Estrov, H. Kantarjian, H. Yang, W.M. Newsome, W.H. Miller, C. Rousseau, A. Kalita, C. Bonfils, M. Dubay, T.A. Patterson, Z. Li, J.M. Besterman, G. Reid, E. Laille, R.E. Martell, M. Minden, Phase 1 study of the oral isotype specific histone deacetylase inhibitor MGCD0103 in leukemia, Blood, 112 (2008) 981-989.
[12] A.M. Evens, S. Balasubramanian, J.M. Vose, W. Harb, L.I. Gordon, R. Langdon, J. Sprague, M. Sirisawad, C. Mani, J. Yue, Y. Luan, S. Horton, T. Graef, N.L. Bartlett, A Phase I/II Multicenter, Open-Label Study of the Oral Histone Deacetylase Inhibitor Abexinostat in Relapsed/Refractory Lymphoma, Clin. Cancer Res., 22 (2016) 1059-1066.
[13] J.H. Tan, S.D. Cang, Y.H. Ma, R.L. Petrillo, D.L. Liu, Novel histone deacetylase inhibitors in clinical trials as anti-cancer agents, J. Hematol. Oncol., 3 (2010).
[14] G. Finazzi, A.M. Vannucchi, V. Martinelli, M. Ruggeri, F. Nobile, G. Specchia, E.M. Pogliani, O.M. Olimpieri, G. Fioritoni, C. Musolino, D. Cilloni, P. Sivera, G. Barosi, M.C. Finazzi, S. Di Tollo, T. Demuth, T. Barbui, A. Rambaldi, A phase II study of Givinostat in combination with hydroxycarbamide in patients with polycythaemia vera unresponsive to hydroxycarbamide monotherapy, Brit. J. Haematol., 161 (2013) 688-694.
[15] D.T. Vogl, N. Raje, S. Jagannath, P. Richardson, P. Hari, R. Orlowski, J.G. Supko, D. Tamang, M. Yang, S.S. Jones, C. Wheeler, R.J. Markelewicz, S. Lonial, Ricolinostat, the First Selective Histone Deacetylase 6 Inhibitor, in Combination with Bortezomib and Dexamethasone for Relapsed or Refractory Multiple Myeloma, Clin. Cancer Res., 23 (2017) 3307-3315.
[16] M. Slingerland, H.J. Guchelaar, H. Gelderblom, Histone deacetylase inhibitors: an overview of the clinical studies in solid tumors, Anti-Cancer Drugs, 25 (2014) 140-149.
[17] Z.Q. Ning, Z.B. Li, M.J. Newman, S. Shan, X.H. Wang, D.S. Pan, J. Zhang, M. Dong, X. Du, X.P. Lu, Chidamide (CS055/HBI-8000): a new histone deacetylase inhibitor of the benzamide class with antitumor activity and the ability to enhance immune cell-mediated tumor cell cytotoxicity, Cancer. Chemother. Pharmacol., 69 (2012) 901-909.
[18] O. Bruserud, C. Stapnes, E. Ersvaer, B.T. Gjertsen, A. Ryningen, Histone deacetylase inhibitors in cancer treatment: A review of the clinical toxicity and the modulation of gene expression in cancer cells, Curr. Pharm. Biotechnol., 8 (2007) 388-400.
[19] E.A. Thomas, Focal nature of neurological disorders necessitates isotype-selective histone deacetylase (HDAC) inhibitors, Mol. Neurobiol., 40 (2009) 33-45.
[20] M. Guha, HDAC inhibitors still need a home run, despite recent approval, Nat. Rev. Drug. Discov., 14 (2015) 226-227.
[21] G.I. Aldana-Masangkay, K.M. Sakamoto, The Role of HDAC6 in Cancer, J. Biomed. Biotechnol., (2011) doi: 10.1155/2011/875824.
[22] K.V. Woan, M. Lienlaf, P. Perez-Villaroel, C. Lee, F. Cheng, T. Knox, D.M. Woods, K. Barrios, J. Powers, E. Sahakian, H.W. Wang, J. Canales, D. Marante, K.S.M. Smalley, J. Bergman, E. Seto, A. Kozikowski, J. Pinilla-Ibarz, A. Sarnaik, E. Celis, J. Weber, E.M. Sotomayor, A. Villagra, Targeting histone deacetylase 6 mediates a dual anti-melanoma effect: Enhanced antitumor immunity and impaired cell proliferation, Mol. Oncol., 9 (2015) 1447-1457.
[23] C. Seidel, M. Schnekenburger, M. Dicato, M. Diederich, Histone deacetylase 6 in health and disease, Epigenomics, 7 (2015) 103-118.
[24] Y. Zhang, N. Li, C. Caron, G. Matthias, D. Hess, S. Khochbin, P. Matthias, HDAC-6 interacts with and deacetylates tubulin and microtubules in vivo, Embo J., 22 (2003) 1168-1179.
[25] S.J. Haggarty, K.M. Koeller, J.C. Wong, C.M. Grozinger, S.L. Schreiber, Domain-selective small-molecule inhibitor of histone deacetylase 6 (HDAC6)-mediated tubulin deacetylation, Proc Natl Acad Sci U S A, 100 (2003) 4389-4394.
[26] O. Witt, H.E. Deubzer, T. Milde, I. Oehme, HDAC family: What are the cancer relevant targets?, Cancer Lett., 277 (2009) 8-21.
[27] Y. Hai, S.A. Shinsky, N.J. Porter, D.W. Christianson, Histone deacetylase 10 structure and molecular function as a polyamine deacetylase, Nat Commun, 8 (2017) 15368.

[28] A. Lahm, C. Paolini, M. Pallaoro, M.C. Nardi, P. Jones, P. Neddermann, S. Sambucini, M.J. Bottomley, P. Lo Surdo, A. Carfi, U. Koch, R. De Francesco, C. Steinkuhler, P. Gallinari, Unraveling the hidden catalytic activity of vertebrate class IIa histone deacetylases, Proc Natl Acad Sci U S A, 104 (2007) 17335-17340.
[29] V. Gaur, T. Connor, A. Sanigorski, S.D. Martin, C.R. Bruce, D.C. Henstridge, S.T. Bond, K.A. McEwen, L. Kerr-Bayles, T.D. Ashton, C. Fleming, M. Wu, L.S. Pike Winer, D. Chen, G.M. Hudson, J.W.R. Schwabe, K. Baar, M.A. Febbraio, P. Gregorevic, F.M. Pfeffer, K.R. Walder, M. Hargreaves, S.L. McGee, Disruption of the Class IIa HDAC Corepressor Complex Increases Energy Expenditure and Lipid Oxidation, Cell Rep, 16 (2016) 2802-2810.
[30] X.X. Wang, R.Z. Wan, Z.P. Liu, Recent advances in the discovery of potent and selective HDAC6 inhibitors, Eur. J. Med. Chem., (2017) doi: 10.1016/j.ejmech.2017.1010.1040.
[31] R. De Vreese, N. Van Steen, T. Verhaeghe, T. Desmet, N. Bougarne, K. De Bosscher, V. Benoy, W. Haeck, L. Van Den Bosch, M. D'Hooghe, Synthesis of benzothiophene-based hydroxamic acids as potent and selective HDAC6 inhibitors, Chem. Commun. (Camb), 51 (2015) 9868-9871.
[32] R. De Vreese, L. Galle, Y. Depetter, J. Franceus, T. Desmet, K. Van Hecke, V. Benoy, L. Van Den Bosch, M. D'Hooghe, Synthesis of Potent and Selective HDAC6 Inhibitors Bearing a Cyclohexane- or Cycloheptane-Annulated 1,5-Benzothiazepine Scaffold, Chemistry, 23 (2017) 128-136.
[33] L. Santo, T. Hideshima, A.L. Kung, J.C. Tseng, D. Tamang, M. Yang, M. Jarpe, J.H. van Duzer, R. Mazitschek, W.C. Ogier, D. Cirstea, S. Rodig, H. Eda, T. Scullen, M. Canavese, J. Bradner, K.C. Anderson, S.S. Jones, N. Raje, Preclinical activity, pharmacodynamic, and pharmacokinetic properties of a selective HDAC6 inhibitor, ACY-1215, in combination with bortezomib in multiple myeloma, Blood, 119 (2012) 2579-2589.
[34] M. Brindisi, C. Cavella, S. Brogi, A. Nebbioso, J. Senger, S. Maramai, A. Ciotta, C. Iside, S. Butini, S. Lamponi, E. Novellino, L. Altucci, M. Jung, G. Campiani, S. Gemma, Phenylpyrrole-based HDAC inhibitors: synthesis, molecular modeling and biological studies, Future Med. Chem., 8 (2016) 1573-1587.
[35] K. Cheng, S. Li, C. Liao, Progress in the Discovery of Macrocyclic Histone Deacetylase Inhibitors for the Treatment of Cancer, Curr Med Chem, 24 (2017) 4166-4179.
[36] Y. Yang, X.Q. Hu, Q.S. Li, X.X. Zhang, B.F. Ruan, J. Xu, C. Liao, Metalloprotein Inhibitors for the Treatment of Human Diseases, Curr Top Med Chem, 16 (2016) 384-396.
[37] Y. Hai, D.W. Christianson, Histone deacetylase 6 structure and molecular basis of catalysis and inhibition, Nat. Chem. Biol., 12 (2016) 741-747.
[38] Y. Miyake, J.J. Keusch, L. Wang, M. Saito, D. Hess, X. Wang, B.J. Melancon, P. Helquist, H. Gut, P. Matthias, Structural insights into HDAC6 tubulin deacetylation and its selective inhibition, Nat Chem Biol, 12 (2016) 748-754.
[39] C.M. Marson, New and unusual scaffolds in medicinal chemistry, Chem. Soc. Rev., 40 (2011) 5514-5533.
[40] Y.J. Zheng, C.M. Tice, The utilization of spirocyclic scaffolds in novel drug discovery, Expert Opin Drug Discov, 11 (2016) 831-834.
[41] M. Benabdallah, O. Talhi, F. Nouali, N. Choukchou-Braham, K. Bachari, A.M.S. Silva, Advances in spirocyclic hybrids: chemistry and medicinal actions, Curr Med Chem, (2018) doi: 10.2174/0929867325666180309124821.
[42] G. Muller, T. Berkenbosch, J.C. Benningshof, D. Stumpfe, J. Bajorath, Charting Biologically Relevant Spirocyclic Compound Space, Chemistry, 23 (2017) 703-710.
[43] D.F. Veber, S.R. Johnson, H.Y. Cheng, B.R. Smith, K.W. Ward, K.D. Kopple, Molecular properties that influence the oral bioavailability of drug candidates, J. Med. Chem., 45 (2002) 2615-2623.
[44] M. Aldeghi, S. Malhotra, D.L. Selwood, A.W. Chan, Two- and three-dimensional rings in drugs, Chem. Biol. Drug. Des., 83 (2014) 450-461.

[45] T.J. Ritchie, S.J. Macdonald, The impact of aromatic ring count on compound developability--are too many aromatic rings a liability in drug design?, Drug Discov. Today, 14 (2009) 1011-1020.
[46] F. Lovering, J. Bikker, C. Humblet, Escape from flatland: increasing saturation as an approach to improving clinical success, J. Med. Chem., 52 (2009) 6752-6756.
[47] F. Lovering, Escape from Flatland 2: complexity and promiscuity, MedChemComm, 4 (2013) 515-519.
[48] Y. Zheng, C.M. Tice, S.B. Singh, The use of spirocyclic scaffolds in drug discovery, Bioorg. Med. Chem. Lett., 24 (2014) 3673-3682.
[49] N.J. Porter, A. Mahendran, R. Breslow, D.W. Christianson, Unusual zinc-binding mode of HDAC6-selective hydroxamate inhibitors, Proc Natl Acad Sci U S A, 114 (2017) 13459-13464.
[50] M.K.W. Mackwitz, A. Hamacher, J.D. Osko, J. Held, A. Scholer, D.W. Christianson, M.U. Kassack, F.K. Hansen, Multicomponent Synthesis and Binding Mode of Imidazo[1,2- a]pyridine-Capped Selective HDAC6 Inhibitors, Org Lett, 20 (2018) 3255-3258.
[51] K.G. Liu, J.R. Lo, A.J. Robichaud, One-pot synthesis of highly substituted indolines, Tetrahedron, 66 (2010) 573-577.
[52] K.G. Liu, A.J. Robichaud, J.R. Lo, J.F. Mattes, Y. Cai, Rearrangement of 3,3-disubstituted indolenines and synthesis of 2,3-substituted indoles, Org. Lett., 8 (2006) 5769-5771.
[53] K.G. Liu, A.J. Robichaud, Synthesis of 3,3-disubstituted oxindoles, Tetrahedron Lett., 48 (2007) 461-463.
[54] B. Heltweg, J. Trapp, M. Jung, In vitro assays for the determination of histone deacetylase activity, Methods, 36 (2005) 332-337.
[55] A. Chakrabarti, I. Oehme, O. Witt, G. Oliveira, W. Sippl, C. Romier, R.J. Pierce, M. Jung, HDAC8: a multifaceted target for therapeutic interventions, Trends Pharmacol Sci, 36 (2015) 481-492.
[56] D. Lagorce, O. Sperandio, J.B. Baell, M.A. Miteva, B.O. Villoutreix, FAF-Drugs3: a web server for compound property calculation and chemical library design, Nucleic Acids Res., 43 (2015) W200-207.
[57] G. Chemi, S. Gemma, G. Campiani, S. Brogi, S. Butini, M. Brindisi, Computational Tool for Fast in silico Evaluation of hERG K+ Channel Affinity, Front. Chem., 5 (2017) 7.
[58] X. Zhang, Z. Yuan, Y. Zhang, S. Yong, A. Salas-Burgos, J. Koomen, N. Olashaw, J.T. Parsons, X.J. Yang, S.R. Dent, T.P. Yao, W.S. Lane, E. Seto, HDAC6 modulates cell motility by altering the acetylation level of cortactin, Mol. Cell., 27 (2007) 197-213.
[59] A.K. Ghosh, M. Brindisi, Organic carbamates in drug design and medicinal chemistry, J. Med. Chem., 58 (2015) 2895-2940.
[60] M.K. Jeon, K.M. Lee, I.H. Kim, Y.K. Jang, S.K. Kang, J.M. Lee, K.Y. Jung, J.A. Kumar, S.D. Rhee, W.H. Jung, J.S. Song, M.A. Bae, K.R. Kim, J.H. Ahn, Synthesis and biological evaluation of thienopyrimidine derivatives as GPR119 agonists, Bioorg. Med. Chem. Lett., 24 (2014) 4281-4285.
[61] C.J. Millard, P.J. Watson, I. Celardo, Y. Gordiyenko, S.M. Cowley, C.V. Robinson, L. Fairall, J.W. Schwabe, Class I HDACs share a common mechanism of regulation by inositol phosphates, Mol. Cell., 51 (2013) 57-67.
[62] M. Brindisi, S. Maramai, S. Gemma, S. Brogi, A. Grillo, L.D. Mannelli, E. Gabellieri, S. Lamponi, S. Saponara, B. Gorelli, D. Tedesco, T. Bonfiglio, C. Landry, K.M. Jung, A. Armirotti, L. Luongo, A. Ligresti, F. Piscitelli, C. Bertucci, M.P. Dehouck, G. Campiani, S. Malone, C. Ghelardini, A. Pittaluga, D. Piomelli, V. Di Marzo, S. Butini, Development and Pharmacological Characterization of Selective Blockers of 2-Arachidonoyl Glycerol Degradation with Efficacy in Rodent Models of Multiple Sclerosis and Pain, J. Med. Chem., 59 (2016) 2612-2632.
[63] S. Brogi, S. Giovani, M. Brindisi, S. Gemma, E. Novellino, G. Campiani, M.J. Blackman, S. Butini, In silico study of subtilisin-like protease 1 (SUB1) from different Plasmodium species in complex with peptidyl-difluorostatones and characterization of potent pan-SUB1 inhibitors, J. Mol. Graph. Model., 64 (2016) 121-130.

[64] L. Zaccagnini, S. Brogi, M. Brindisi, S. Gemma, G. Chemi, G. Legname, G. Campiani, S. Butini, Identification of novel fluorescent probes preventing PrPSc replication in prion diseases, Eur. J. Med. Chem., 127 (2017) 859-873.
[65] W.C. Still, A. Tempczyk, R.C. Hawley, T. Hendrickson, Semianalytical Treatment of Solvation for Molecular Mechanics and Dynamics, J. Am. Chem. Soc., 112 (1990) 6127-6129.
[66] M. Brindisi, S. Gemma, S. Kunjir, L. Di Cerbo, S. Brogi, S. Parapini, S. D'Alessandro, D. Taramelli, A. Habluetzel, S. Tapanelli, S. Lamponi, E. Novellino, G. Campiani, S. Butini, Synthetic spirocyclic endoperoxides: new antimalarial scaffolds, MedChemComm, 6 (2015) 357-362.
[67] S. Brogi, A. Fiorillo, G. Chemi, S. Butini, M. Lalle, A. Ilari, S. Gemma, G. Campiani, Structural characterization of Giardia duodenalis thioredoxin reductase (gTrxR) and computational analysis of its interaction with NBDHEX, Eur J Med Chem, 135 (2017) 479-490.
[68] R. Wu, Z. Lu, Z. Cao, Y. Zhang, Zinc chelation with hydroxamate in histone deacetylases modulated by water access to the linker binding channel, J Am Chem Soc, 133 (2011) 6110-6113.
[69] J. Zhou, R. Wu, H.B. Luo, Inhibition mechanism of SAHA in HDAC: a revisit, Phys Chem Chem Phys, 17 (2015) 29483-29488.
[70] S.A. Ganai, Z. Farooq, S. Banday, M. Altaf, In silico approaches for investigating the binding propensity of apigenin and luteolin against class I HDAC isoforms, Future Med Chem, (2018) 10.4155/fmc-2018-0020.
[71] H. Tavakol, Computational study of simple and water-assisted tautomerism of hydroxamic acids, Journal of Molecular Structure-Theochem, 916 (2009) 172-179.
[72] S. Kalyaanamoorthy, Y.P. Chen, Quantum polarized ligand docking investigation to understand the significance of protonation states in histone deacetylase inhibitors, J Mol Graph Model, 44 (2013) 44-53.
[73] J. Pottel, E. Therrien, J.L. Gleason, N. Moitessier, Docking ligands into flexible and solvated macromolecules. 6. Development and application to the docking of HDACs and other zinc metalloenzymes inhibitors, J Chem Inf Model, 54 (2014) 254-265.
[74] A.V. Bieliauskas, S.V. Weerasinghe, A.T. Negmeldin, M.K. Pflum, Structural Requirements of Histone Deacetylase Inhibitors: SAHA Analogs Modified on the Hydroxamic Acid, Arch Pharm (Weinheim), 349 (2016) 373-382.
[75] B. Heltweg, F. Dequiedt, E. Verdin, M. Jung, Nonisotopic substrate for assaying both human zinc and NAD+-dependent histone deacetylases, Anal. Biochem., 319 (2003) 42-48.
[76] D. Wegener, F. Wirsching, D. Riester, A. Schwienhorst, A fluorogenic histone deacetylase assay well suited for high-throughput activity screening, Chem. Biol., 10 (2003) 61-68.
[77] M. Marek, S. Kannan, A.T. Hauser, M. Moraes Mourao, S. Caby, V. Cura, D.A. Stolfa, K. Schmidtkunz, J. Lancelot, L. Andrade, J.P. Renaud, G. Oliveira, W. Sippl, M. Jung, J. Cavarelli, R.J. Pierce, C. Romier, Structural basis for the inhibition of histone deacetylase 8 (HDAC8), a key epigenetic player in the blood fluke Schistosoma mansoni, PLoS Pathog, 9 (2013) e1003645.
[78] T. Heimburg, A. Chakrabarti, J. Lancelot, M. Marek, J. Melesina, A.T. Hauser, T.B. Shaik, S. Duclaud, D. Robaa, F. Erdmann, M. Schmidt, C. Romier, R.J. Pierce, M. Jung, W. Sippl, Structure-Based Design and Synthesis of Novel Inhibitors Targeting HDAC8 from Schistosoma mansoni for the Treatment of Schistosomiasis, J Med Chem, 59 (2016) 2423-2435.
[79] C.A. Schneider, W.S. Rasband, K.W. Eliceiri, NIH Image to ImageJ: 25 years of image analysis, Nat. Methods, 9 (2012) 671-675.
[80] P. Bontempo, D. Rigano, A. Doto, C. Formisano, M. Conte, A. Nebbioso, V. Carafa, G. Caserta, V. Sica, A.M. Molinari, L. Altucci, Genista sessilifolia DC. extracts induce apoptosis across a range of cancer cell lines, Cell. Prolif., 46 (2013) 183-192.
[81] M. Conte, C. Dell'Aversana, R. Benedetti, F. Petraglia, A. Carissimo, V.B. Petrizzi, A.M. D'Arco, C. Abbondanza, A. Nebbioso, L. Altucci, HDAC2 deregulation in tumorigenesis is causally connected to repression of immune modulation and defense escape, Oncotarget, 6 (2015) 886-901.

ACCEPTED MANUSCRIPT

ACCEPTED MANUSCRIPT

ACCEPTED MANUSCRIPT

Highlights

-Rational design of novel spiroindoline as HDAC6 inhibitors

-Biological studies showed a strong antitumor potential for the synthesized compounds

-Compound **5b** was able to potently inhibit cell migration in a SH-SY5Y cell culture

-Compound **5b** did not display toxicity in NIH3T3 mouse fibroblasts

ACCEPTED MANUSCRIPT